



# Ultra-compact mode (de) multiplexer based on subwavelength asymmetric Y-junction

WEIJIE CHANG, LULUZI LU, XINSHU REN, DONGYU LI, ZEPENG PAN,  
MENGFAN CHENG, DEMING LIU, AND MINMING ZHANG\*

<sup>1</sup>School of Optical and Electrical Information, Huazhong University of Science and Technology, Wuhan 430074, China

<sup>2</sup>Wuhan National Laboratory for Optoelectronics, Huazhong University of Science and Technology, Wuhan 430074, China

\*mmz@hust.edu.cn

**Abstract:** We propose and experimentally demonstrate a novel multimode ultra-compact mode (de)multiplexer for highly integrated on-chip mode-division multiplexing systems. This device is composed of a wide divergence angle asymmetric Y-junction based on subwavelength structure and optimized using an inverse design method. The proposed device occupied a footprint of only  $2.4 \times 3 \mu\text{m}^2$ . The measured insertion loss and crosstalk were less than 1dB and -24 dB from 1530 nm to 1590 nm for both  $\text{TE}_0$  mode and  $\text{TE}_1$  mode, respectively. Likewise, a three mode multiplexer is also designed and fabricated with a compact footprint of  $3.6 \times 4.8 \mu\text{m}^2$ . Furthermore, our scheme could also be expanded to include more modes.

© 2018 Optical Society of America under the terms of the [OSA Open Access Publishing Agreement](#)

**OCIS codes:** (130.3120) Integrated optics devices; (060.4230) Multiplexing; (160.3918) Metamaterials.

## References and links

1. L. W. Luo, N. Ophir, C. P. Chen, L. H. Gabrielli, C. B. Poitras, K. Bergmen, and M. Lipson, "WDM-compatible mode-division multiplexing on a silicon chip," *Nat. Commun.* **5**, 3069 (2014).
2. Y. Ding, J. Xu, F. Da Ros, B. Huang, H. Ou, and C. Peucheret, "On-chip two-mode division multiplexing using tapered directional coupler-based mode multiplexer and demultiplexer," *Opt. Express* **21**(8), 10376–10382 (2013).
3. J. Wang, P. Chen, S. Chen, Y. Shi, and D. Dai, "Improved 8-channel silicon mode demultiplexer with grating polarizers," *Opt. Express* **22**(11), 12799–12807 (2014).
4. Z. Zhang, X. Hu, and J. Wang, "On-chip optical mode exchange using tapered directional coupler," *Sci. Rep.* **5**(1), 16072 (2015).
5. T. Uematsu, Y. Ishizaka, Y. Kawaguchi, K. Saitoh, and M. Koshiba, "Design of a Compact Two-Mode Multi/Demultiplexer Consisting of Multimode Interference Waveguides and a Wavelength-Insensitive Phase Shifter for Mode-Division Multiplexing Transmission," *J. Lightwave Technol.* **30**(15), 2421–2426 (2012).
6. M. Ye, Y. Yu, J. Zou, W. Yang, and X. Zhang, "On-chip multiplexing conversion between wavelength division multiplexing-polarization division multiplexing and wavelength division multiplexing-mode division multiplexing," *Opt. Lett.* **39**(4), 758–761 (2014).
7. J. D. Love and N. Riesen, "Single-, few- and multimode Y-Junctions," *J. Lightwave Technol.* **30**(3), 304–309 (2012).
8. N. Riesen and J. D. Love, "Design of mode-sorting asymmetric Y-junctions," *Appl. Opt.* **51**(15), 2778–2783 (2012).
9. J. B. Driscoll, R. R. Grote, B. Souhan, J. I. Dadap, M. Lu, and R. M. Osgood, "Asymmetric Y junctions in silicon waveguides for on-chip mode-division multiplexing," *Opt. Lett.* **38**(11), 1854–1856 (2013).
10. W. Chen, P. Wang, T. Yang, G. Wang, T. Dai, Y. Zhang, L. Zhou, X. Jiang, and J. Yang, "Silicon three-mode (de)multiplexer based on cascaded asymmetric Y junctions," *Opt. Lett.* **41**(12), 2851–2854 (2016).
11. L. F. Frellsen, Y. Ding, O. Sigmund, and L. H. Frandsen, "Topology optimized mode multiplexing in silicon-on-insulator photonic wire waveguides," *Opt. Express* **24**(15), 16866–16873 (2016).
12. A. Y. Piggott, J. Lu, K. G. Lagoudakis, J. Petykiewicz, T. M. Babinec, and J. Vučković, "Inverse design and demonstration of a compact and broadband on-chip wavelength demultiplexer," *Nat. Photonics* **9**(6), 374–377 (2015).
13. B. Shen, P. Wang, R. Polson, and R. Menon, "An integrated-nanophotonics polarization beamsplitter with  $2.4 \times 2.4 \mu\text{m}^2$  footprint," *Nat. Photonics* **9**(6), 378–382 (2015).
14. A. Y. Piggott, J. Lu, T. M. Babinec, K. G. Lagoudakis, J. Petykiewicz, and J. Vučković, "Inverse design and implementation of a wavelength demultiplexing grating coupler," *Sci. Rep.* **4**(1), 7210 (2014).

15. Z. Yu, H. Cui, and X. Sun, "Genetic-algorithm-optimized wideband on-chip polarization rotator with an ultrasmall footprint," Opt. Lett. **42**(16), 3093–3096 (2017).
16. K. Xu, L. Liu, X. Wen, W. Sun, N. Zhang, N. Yi, S. Sun, S. Xiao, and Q. Song, "Integrated photonic power divider with arbitrary power ratios," Opt. Lett. **42**(4), 855–858 (2017).
17. J. C. C. Mak, C. Sideris, J. Jeong, A. Hajimiri, and J. K. S. Poon, "Binary particle swarm optimized  $2 \times 2$  power splitters in a standard foundry silicon photonic platform," Opt. Lett. **41**(16), 3868–3871 (2016).
18. L. Lu, D. Liu, F. Zhou, D. Li, M. Cheng, L. Deng, S. Fu, J. Xia, and M. Zhang, "Inverse-designed single-step-etched colorless 3 dB couplers based on RIE-lag-insensitive PhC-like subwavelength structures," Opt. Lett. **41**(21), 5051–5054 (2016).
19. J. D. Love, R. W. C. Vance, and A. Joblin, "Asymmetric, adiabatic multipronged planar splitters," Opt. Quantum Electron. **28**(4), 353–369 (1996).
20. L. Lalanne and D. Lemercier-Lalanne, "On the effective medium theory of subwavelength periodic structures," J. Mod. Opt. **43**(10), 2063–2085 (1996).
21. L. Lu, M. Zhang, F. Zhou, W. Chang, J. Tang, D. Li, X. Ren, Z. Pan, M. Cheng, and D. Liu, "Inverse-designed ultra-compact star-crossings based on PhC-like subwavelength structures for optical intercross connect," Opt. Express **25**(15), 18355–18364 (2017).
22. Lumerical FDTD solutions, <https://www.lumerical.com>.
23. W. Chang, M. Zhang, L. Lu, F. Zhou, D. Li, Z. Pan, and D. Liu, "Inverse design of an ultra-compact mode (de)multiplexer based on subwavelength structure," in *Conference on Lasers and Electro-Optics*, OSA Technical Digest (Optical Society of America, 2017), paper SF1J.8.

## 1. Introduction

In recent years, mode-division multiplexing (MDM) on silicon-on-insulator (SOI) platform, as a more promising and attractive technology, has shown great potential to further increase the transmission capacity of on-chip optical interconnects [1]. A high performance mode (de)multiplexer ((De) MUX) with compact footprint, low insertion and low crosstalk is an essential component for realizing a densely integrated MDM system. Various MUX schemes based on conventional silicon waveguides have been reported typically including asymmetric directional couplers (ADCs) [2–4], multimode interferometers (MMI) [5, 6], or asymmetric Y-junction [7–10]. Although these schemes have proved to be promising, they usually suffer from a relatively large footprint of tens or hundreds of  $\mu\text{m}^2$  for a two-mode multiplexer. Recently, one used the topology optimization method to design free-formed waveguide structure to decrease the scale of devices to several microns [11]. It exhibited high performance for two-mode MUXs. Unfortunately, the crosstalk for the three-mode MUX reached  $-12$  dB. A mode multiplexer with compact footprint and excellent performance is highly desired for dense photonic integrated circuits.

Due to its broad bandwidth and unique mode-sorting characteristics, the asymmetric Y-junction based on conventional waveguides has been utilized to realize multimode MUX. Unfortunately, the footprint of this structure is usually quite large (hundreds of microns) because small branching angle ( $< 9^\circ$ ) is required for satisfying adiabatic evolution [9]. Recently, free-form or digital silicon subwavelength (SW) structures enable one to manipulate light field at the nanoscale, and have shown great potential to realize ultra-compact and highly functional devices simultaneously [12–17]. However, silicon components based on inverse-designed SW structures usually have complex etching patterns. The feature sizes of tiny holes in one such pattern may vary randomly and dramatically, leading to unpredictable fabrication error (non-uniformity of holes' etched depths) due to the reactive ion etching lag effect. To relax the fabrication tolerance, we proposed a PhC-like SW structure earlier which could suppress such fabrication error caused by the lag effect [18]. Although these inverse-designed nanophotonic devices may exhibit high performance, it seems difficult to explore their working mechanisms as we do to the conventional waveguide devices.

In this work, we propose a novel multimode ultra-compact mode (de) multiplexer composed of asymmetric Y-junction based on the PhC-like SW structure using the inverse design method. By optimizing the circular holes' combination in the inverse design region, we can flexibly engineer the refractive index distribution at the nanoscale to realize equivalent wide-angle asymmetric Y-junctions to (de)multiplex two or more modes. In this

way, the footprint of the proposed device is two orders of magnitude smaller than that of conventional waveguide-based Y-junction. The fabricated two-mode and three-mode MUXs occupied  $2.4 \times 3 \mu\text{m}^2$  and  $3.6 \times 4.8 \mu\text{m}^2$ , respectively. The measured crosstalk of these two types of MUXs were  $-24 \text{ dB}$  and  $-19 \text{ dB}$  respectively.

## 2. Design, optimization and simulations

Figure 1(a) shows a two-mode (De) MUX based on conventional waveguide asymmetric Y-junction. Due to the closest effective refractive index of the local modes in the stem and arms, the TE<sub>0</sub> and TE<sub>1</sub> modes in the input stem waveguide could evolve into two local fundamental modes in the two branches respectively. Notably, the cross-sectional variation at the junction is sufficiently small to ensure approximately adiabatic behavior. Thus, a small divergence angle is required, which results in an extremely large scale of the Y-junction. For multi-arm asymmetric Y-junctions with multiple modes, as shown in Fig. 1(b), the length of the Y-junction is approximately proportional to the fourth power of the number of modes [19]. A mode conversion factor (MCF) is used to evaluate the effect of mode conversion, defined as [5]:

$$\text{MCF} = \frac{2|\beta_1 - \beta_2|}{\tan \theta \cdot \left[ (\beta_1 + \beta_2)^2 - (2n_0 k)^2 \right]^{1/2}} \quad (1)$$

where  $\beta_1$  and  $\beta_2$  are the propagation constants of the local fundamental modes in the two arms respectively,  $\theta$  is the divergence angle,  $n_0$  is the refractive index between the arms and is the free-space wave-number. Mode conversion occurs when the MCF is greater than approximately 0.43, providing a transition boundary between mode-separation and power-splitting [8].

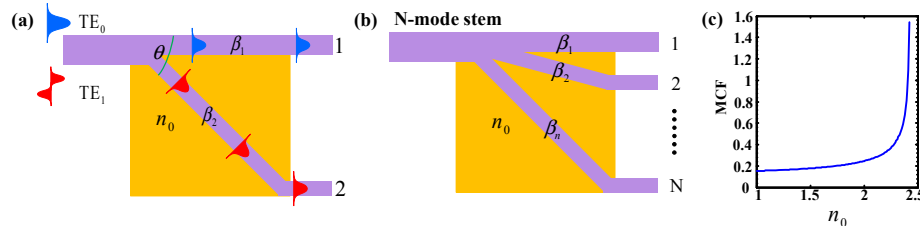


Fig. 1. (a) and (b)Working principles for two-mode (De) MUX and N-mode (De) MUX based on conventional waveguides and asymmetric Y-junctions, respectively. (c) Mode conversion factor (MCF) as a function of the refractive index of the material.

Here, we take the two-mode MUX as an example for detailed description. In the case of maintaining the gap between two output arms at least  $1 \mu\text{m}$ , the larger the divergence angle  $\theta$  is, the smaller the scale of MUX is. For a MUX based on a conventional Y-junction, we assume that the cross sections of arm 1 and arm 2 are  $220 \times 550 \text{ nm}^2$  and  $220 \times 450 \text{ nm}^2$  respectively. The corresponding propagation constants  $\beta_1$  and  $\beta_2$  are  $10.54 \mu\text{m}^{-1}$  and  $9.16 \mu\text{m}^{-1}$  at the wavelength of  $1550 \text{ nm}$ . If we set  $\theta = 45^\circ$ ,  $n_0$  should be larger than 2.3 according to Eq. (1), as illustrated in Fig. 1(c). Apparently, it cannot be achieved for conventional air-cladded or SiO<sub>2</sub>-cladded waveguides based on the simple single-step-etching process. In our work, the PhC-like structure provides an additional design degree of freedom to design wide-angle asymmetric Y-junctions for mode conversion could be achieved by the PhC-like SW structure. Furthermore, free-form PhC-like SW structures could manipulate the phase profile

of an optical field with a high degree of freedom at the nanoscale [21]. So the diffraction loss of a wide-angle Y-junction based on the PhC-like SW structure could be minimized using proper inverse design method. In this way, we can utilize the PhC-like SW structure to realize ultra-compact and highly functional two-mode MUX simultaneously.

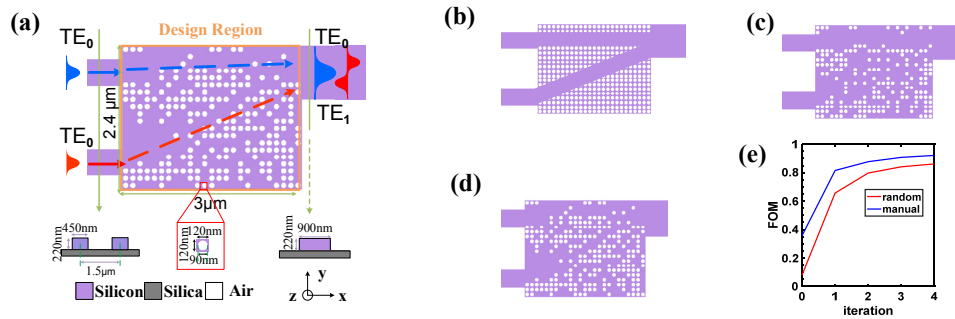


Fig. 2. (a) Schematic of the two-mode MUX based on SW structure asymmetric Y-junction. (b) The manual initial pattern of inverse design region for two-mode MUX. (c) and (d) The optimized patterns for random and manually-set initials, respectively. (e) The calculated FOMs after every iteration for manually-set and random initial patterns.

As shown in Fig. 2(a), the proposed two mode MUX based on the PhC-like SW structure is designed on a silicon-on-insulator platform with 220 nm-thick air-cladded top silicon layer. The inverse design region composed of  $20 \times 25$  discrete pixels occupies a compact footprint of only  $2.4 \times 3 \mu\text{m}^2$ . Each pixel is a square of  $120 \times 120 \text{ nm}^2$  with a circular hole. The hole has a radius of 45 nm and a depth of 220 nm. According to the effective medium theory [20], the effective material refractive index of our proposed PhC-like SW structure with air hole is 2.38. Each pixel has two states: ‘0’ represents a fully etched hole and ‘1’ represents that the hole is not etched. The widths of the two input waveguides and the output waveguide are 450 nm and 900 nm, respectively. The gap between the two input waveguides should be more than 1  $\mu\text{m}$  to avoid unwanted coupling.

Considering that inverse design may be sensitive to the initial pattern, we also set different types of initial patterns. A manually-set initial pattern like a Y-junction is designed as shown in Fig. 1(b) and a random initial pattern is also generated for comparison and analysis. Our simulation results indicate that the device with manually-set initial pattern usually exhibits better performance than that with random initial pattern. The figure-of-merit (FOM) of the device for inverse design is defined as:

$$\text{FOM} = 1 - (1 - \alpha) \cdot \frac{1}{2M} \cdot \sum (|1 - t_1| + |1 - t_2|) - \alpha \cdot \frac{1}{2M} \sum (x_1 + x_2) \quad (2)$$

where  $t_1$  and  $t_2$  are the transmittance of input1  $TE_0$ -output  $TE_0$  and the mode converting efficiency of input2  $TE_0$ -output  $TE_1$  via inverse design region, respectively. Likewise,  $x_1$  and  $x_2$  are the transmittance of input1  $TE_0$ -output  $TE_1$  and input2  $TE_0$ -output  $TE_0$ , respectively.  $M$  denotes the number of wavelength channels. Three wavelengths over an operating bandwidth of 80 nm are taken into consideration in simulations. Actually, the second term in the right of Eq. (2) is used to optimize average insertion loss (IL) and the third one is employed to minimize the crosstalk (CT).  $\alpha$ , a weighted coefficient over a range from 0 to 1, is utilized to achieve a tradeoff between IL and CT of the device. For an ideal two mode MUX, the FOM is 1.

The nonlinear direct-binary-search (DBS) optimization algorithm is utilized to design the local optimum hole combinations. The method is described in detail in [13]. In general, we randomly chose one pixel to toggle its state, and calculate the FOM using a 3D finite-difference time-domain method via a commercial software (Lumerical FDTD Solutions) [22].

If the FOM increases, then the reversed pixel state will be reserved. Otherwise, the pixel goes back to the original state. One iteration ends up with all pixels traversed. When the FOM exhibits no great improvement after one iteration (< 1% for our case), the whole optimization will end. In the initial step of the optimization process,  $\alpha$  is set to 0 in order to achieve quite low IL. Subsequently, by designing appropriate  $\alpha$ , a low IL and low CT of the compact device could be realized.

It takes about 36 hours to get the optimized nanopattern on a computer with an 8-core central processing unit (Intel Xeon E5-2637). Figures 2(c) and 2(d) show the optimized patterns for the manually-set initial pattern given in Fig. 2(b) and random initial pattern with the same FOM, respectively. The calculated FOMs for the manually-set and random initial patterns after 4 iterations are illustrated in Fig. 2(e). The FOM for the manually-set initial pattern is usually greater than that for random initial pattern, which means an appropriate initial pattern provides an effective approach to achieve higher performance.

As illustrated in Figs. 3(a) and 3(b), the working mechanism of the compact SW MUX is equivalent to that of the conventional waveguide MUX based on asymmetric Y-junction in Fig. 1(a), while the footprint of the subwavelength scheme is reduced by about 100 times. The compact SW structure asymmetric Y-junction converts  $TE_0$  and  $TE_1$  in the wide stem waveguide to the corresponding local fundamental modes with a large divergence angle. As mentioned before, the PhC-like SW structure provides an effective approach to engineering the material index between two arms and enable MCF to be still greater than 0.43 to realize a wide divergence angle. The simulated ILs for both  $TE_0$  and  $TE_1$  are less than 0.47 dB and the CTs are lower than -24 dB from 1530 to 1590 nm, as given in Fig. 3(c). Furthermore, the simulation results of the MDM system composed of a MUX and a DeMUX are also shown in Fig. 3(d). The simulated ILs for both  $TE_0$  and  $TE_1$  are less than 0.91 dB and the CTs are lower than -24 dB over an operating bandwidth of 60 nm centered at 1560 nm.

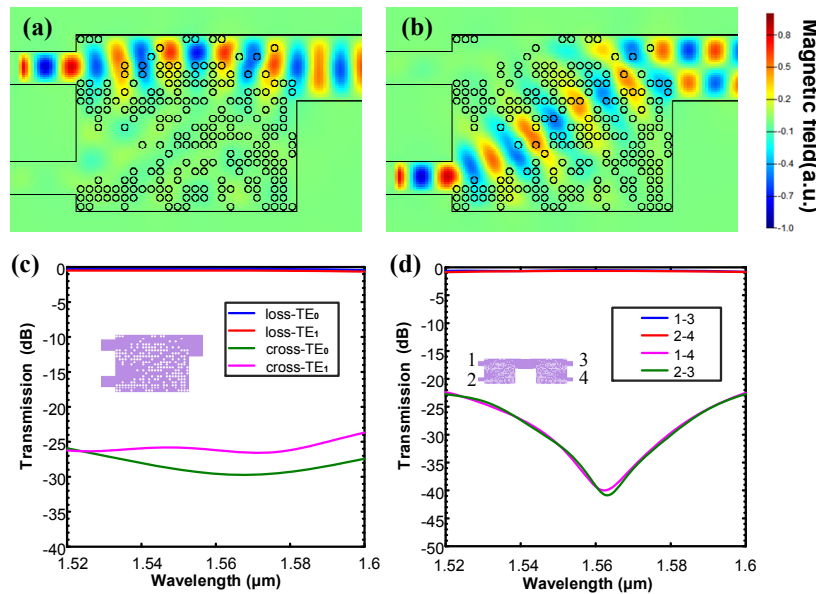


Fig. 3. (a) and (b) Simulated magnetic field distribution of Hz for  $TE_0$  and  $TE_1$ , respectively.  
(c) and (d) Simulated spectra transmission for the MUX and the MDM system, respectively.

### 3. Experiment results

The proposed compact MUX based on a SW structure asymmetric Y-junction was fabricated using an electron-beam lithography (EBL) system (Vistec EBLG 5000 Plus) to form the optimum pattern on a SOI platform with a 220 nm thick top silicon layer, and an inductively

coupled plasma (ICP) etcher (Plasmalab System100) to transfer the mask to the silicon device layer. Due to lag effect, when the strip waveguides were just fully etched (220nm), the etch depth of the circular holes with radii of 45 nm was approximately 140 nm. As a result, the etching time was increased to ensure the full etching of the nanopattern [23].

The top-view scanning electron microscope (SEM) pictures of MDM system and the referenced grating coupler are illustrated in Fig. 4(a). Figures 4(b) and 4(c) show the detailed SEM images of the fabricated MDM system and MUX, respectively. From the spectral transmission scans for each combination of input and output ports, we can characterize the fabricated two-mode MUX. A broad amplified spontaneous emission (ASE) light source with an operating bandwidth of 80 nm centered at 1560 nm and an optical spectrum analyzer (Yokogawa AQ6370C-20) were utilized to measure the spectral transmission. Our fabricated device only occupied a footprint of  $2.4 \times 3 \mu\text{m}^2$  benefiting from a wide divergence angle. The measured ILs for both  $\text{TE}_0$  and  $\text{TE}_1$  were less than 1 dB and the CTs were lower than -24 dB with an operating bandwidth of 60nm. The experimental results had a great agreement with our simulations.

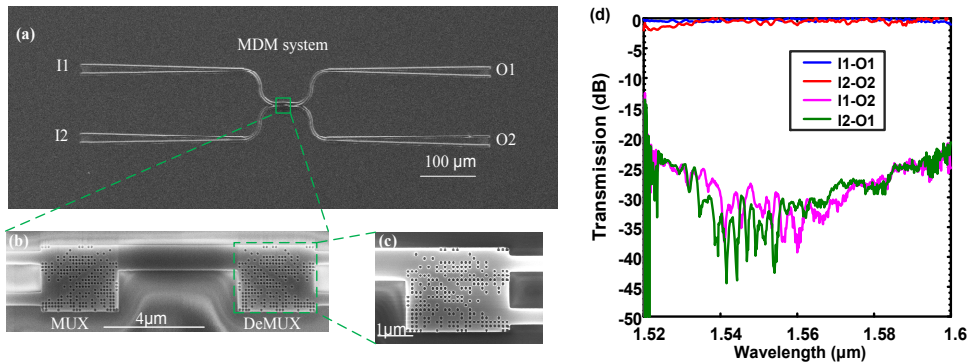


Fig. 4. (a) SEM image for the fabricated MDM system (b) and (c) The detailed SEM pictures for the MDM system with a 5  $\mu\text{m}$  long bus waveguide and the DeMUX, respectively. (d) The measured spectrum transmission for the fabricated MDM link

#### 4. Three-mode multiplexer

To verify the functionality and extendibility of our proposed equivalent model based on SW structure asymmetric Y-junction, we designed, fabricated and experimentally demonstrated a three mode MUX with a similar optimization method and a fabrication process identical to the one described for the two mode MUX. As shown in Fig. 5(a), the device is composed of three single mode waveguides, a multimode waveguide supporting three modes and an inverse design with  $30 \times 40$  pixels. The manually-set initial pattern combinations were also quite similar to an asymmetric Y-junction, which was expected to achieve higher performance than random initial pattern combinations. Under the circumstances of the similar optimization method present for two-mode MUX, the optimized pattern is obtained as given in Fig. 5(b). Meanwhile, the corresponding magnetic profiles of  $\text{TE}_0$ ,  $\text{TE}_1$  and  $\text{TE}_2$  are illustrated in Figs. 5(c) and 5(d), respectively. As expected, the local fundamental modes launched in different input waveguides were converted to the corresponding higher order modes via a SW structure asymmetric Y-junction with a wide divergence angle.

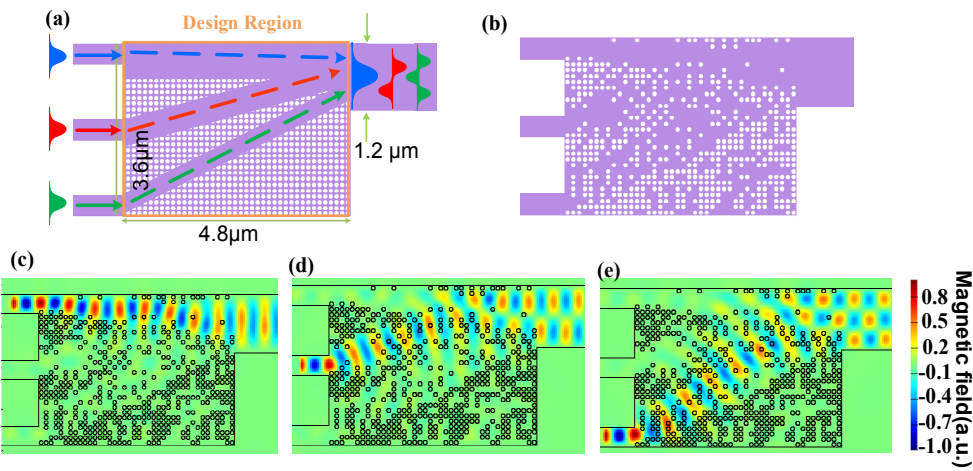


Fig. 5. (a) Schematic of the two-mode MUX based on SW structure asymmetric Y-junction. (b) The optimized pattern for the manually-set initial pattern as shown in Fig. 5(a). (c)- (e) Simulated magnetic field distributions of Hz for TE<sub>0</sub>, TE<sub>1</sub> and TE<sub>2</sub>, respectively.

The MDM system for three modes was fabricated with the same condition as the two-mode MUX and was utilized to verify its performance and functionality. Figures 6(a) and 6(b) show the SEM images for MDM link and DeMUX, respectively. As given in Figs. 6(c) and 6(d), spectra for all possible paths of the light injected in the upper, middle and lower input waveguides were measured over a wavelength range from 1520 nm to 1600 nm. The measured ILs and CTs for both TE<sub>0</sub> and TE<sub>1</sub> were less than 1.2 dB and -22 dB, respectively. For TE<sub>2</sub>, the measured IL was less than 2.5 dB and the CT was lower than -19 dB with an operating width of 60 nm centered at 1560 nm. Our simulation and experimental results indicate the MUX based on SW asymmetric Y-junction is well suitable for multimode and still exhibits high performance without a substantial increase in the device footprint. We believe it shows great potential in densely integrated photonic circuit applications.

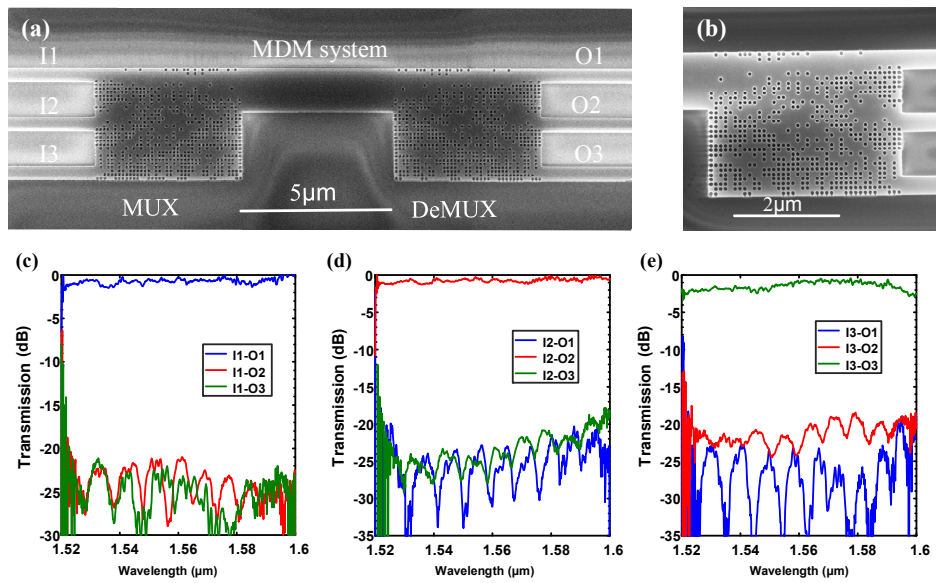


Fig. 6. (a) SEM image for the fabricated three- mode MDM system (b) the detailed SEM picture for DeMUX. (c)- (e) The measured spectra transmission for TE<sub>0</sub> injected in the upper, middle, lower input waveguides, respectively.

## 5. Discussion

To further investigate the fabrication tolerance of the proposed structure, we modified the radii of etching holes from 40 to 50 nm and simulated the performance of the two-mode and three-mode MUXs with the previously optimized patterns, respectively. Figures 7(a)-7(d) show the simulated ILs and CTs of  $TE_0$  and  $TE_1$  for the two-mode MUX with different holes' radii, respectively. The simulated ILs for both modes increase about 1 dB in average for  $\pm 5$  nm radii variation, compared with the device with a void radius of 45 nm. The simulated average degradation of CTs is less than 7 dB for both modes. In addition, the average transmission profiles of  $TE_0$ ,  $TE_1$  and  $TE_2$  for the three-mode MUX as functions of holes' radii are presented in Figs. 7(e)-7(f), respectively. Specifically, we can find that the  $TE_2$  mode of the three-mode MUX exhibits an obvious deterioration when the holes' radius is larger than 45 nm, which probably occurs to an over etching device. We may estimate the ICP etching velocity before etching the device and avoid over etching by setting an appropriate etching time. We also fabricated the proposed three-mode MUX in this way.

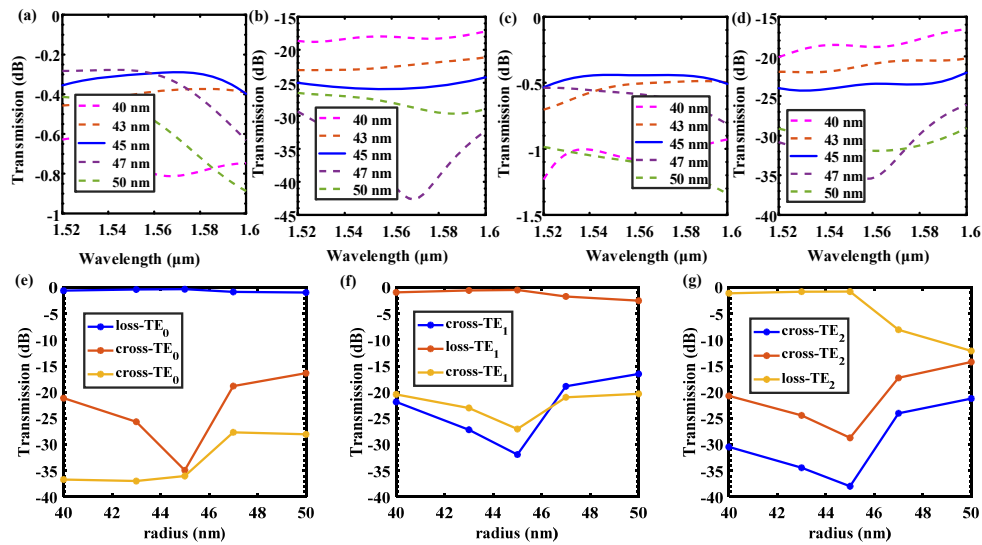


Fig. 7. (a) and (b) Simulated ILs and CTs of  $TE_0$  for the two-mode MUX with different holes radii varying from 40 nm to 50 nm, respectively. (c) and (d) Simulated ILs and CTs of  $TE_1$  for the two-mode MUX with different holes radii varying from 40 nm to 50 nm, respectively. (e)-(g) Simulated average transmission of  $TE_0$ ,  $TE_1$  and  $TE_2$  for the three-mode MUX as a function of various holes radii, respectively.

Furthermore, the proposed three-mode MUX based on the PhC-like SW structure has an approximately 10 dB better CT than that based on the topology optimization structure in [11]. We think that there are two possible reasons for such results. Firstly, the three-mode MUX based on the PhC-like SW structure may suffer from fabrication errors less than that in [11] does. Our simulation results show that the performance of the three-mode MUX is sensitive to fabrication errors compared with the two-mode one. The lag effect is one of dominant fabrication errors in single step plasma etching processes [18]. Fortunately, the PhC-like SW structure can eliminate the random changes of feature sizes of etching holes and offer an outstanding lag-effect-insensitive feature in the single step plasma etching processes, compared with other SW structures which consist of holes with random feature sizes. Secondly, a proper initial pattern may help to approach the global optimization during the inverse design process. Our simulation results show that the proposed MUXs work like equivalent asymmetric Y-junctions. To ease the sensitivity of optimal performance to the initial pattern, we manually set the initial pattern like an asymmetric Y-junction and we find

that a Y-junction-like initial pattern usually results in a better performance than a random one does, as shown in Fig. 2(e).

## 6. Conclusion

In summary, we have proposed and experimentally demonstrated an ultra-compact multimode MUX based on the SW structure asymmetric Y-junction using the inverse design method. By engineering material index and manipulating phase profiles of light at the nanoscale, we realize SW structure asymmetric Y-junctions with large divergence angles to reduce the device footprint. The footprint of the fabricated two-mode MUX was  $2.4 \times 3 \mu\text{m}^2$ , which is two orders of magnitude smaller than that of conventional one. The measured ILs for both  $\text{TE}_0$  and  $\text{TE}_1$  modes were less than 1 dB and the measured CTs were lower than -24 dB from 1530 nm to 1590 nm. In addition, a three mode MUX was also designed and fabricated with the identical method. It also exhibited high performance with a compact footprint of  $3.6 \times 4.8 \mu\text{m}^2$ , and the measured CT was lower than -19 dB over an operating bandwidth of 60 nm. Our simulation and experimental results indicate that the proposed scheme could be expanded to design MUXs supporting more modes. The proposed ultra-compact (De) MUXs may offer an effective approach to promote practical applications of densely integrated photonic MDM systems for on-chip optical interconnection.

## Funding

National Natural Science Foundation of China (61775069).